International Journal of Biological Macromolecules 101 (2017) 896–903

Contents lists available at ScienceDirect

International Journal of Biological Macromolecules

journal homepage: www.elsevier.com/locate/ijbiomac

Detection of glycated hemoglobin with voltammetric sensing amplified by 3D-structured nanocomposites

Utkarsh Jain, Shaivya Gupta, Nidhi Chauhan*

Amity Institute of Nanotechnology, Amity University, Noida 201303, Uttar Pradesh, India

ARTICLE INFO

Article history:
Received 1 February 2017
Received in revised form 19 March 2017
Accepted 22 March 2017
Available online 30 March 2017

Keywords:
Glycated hemoglobin
Graphene oxide (rGO)
Multiwalled carbon nanotubes (MWCNT) and platinum nanoparticles
Fructosyl valine oxidase

ABSTRACT

Glycated hemoglobin (HbA1c), a marker for glycine level in blood, while detecting over a long period of time (up to 2–3 months) shows consistency. Therefore, HbA1c has been mostly used and indeed an established test for monitoring the glycemic control in persons suffering from diabetes. 3D-structured reduced graphene oxide (rGO), multiwalled carbon nanotubes (MWCNT) and platinum nanoparticles (PtNPs) composite (PtNPs/rGO–MWCNT) were synthesized and used as interface for the development of an electrochemical HbA1c biosensor. The network structure of rGO–MWCNT nanocomposite provides more active sites for Pt deposition and the synergistic effect of rGO, MWCNTs and PtNPs significantly improved the electrochemical performance of the working electrode. The structure of PtNPs/rGO–MWCNT nanocomposite was characterized by scanning electron microscopy (SEM), cyclic voltammetry (CV) and electrochemical impedance study (EIS). This biosensor exhibited a response time of less than 3 s, a wide linear concentration range of 0.05–1000 μM with detection limit of 0.1 μM, good repeatability and satisfactory reproducibility. The biosensor retained 50% of its initial response after 12 weeks at 25 °C. The proposed biosensor was successfully applied for the determination of HbA1c concentration in human blood samples with recoveries between 93.7 and 98.3%.

1. Introduction

Nanocomposites have expectantly an intense research field mainly in biosensor fabrication in most recent years considering their potential applications for bioassays [1,2]. For utilization in the fabrication of biosensors, a wide range of nanomaterials such as gold, silver [3], carbon nanotubes (CNTs), thallium(III) oxide (Tl_2O_3) [4–6], aluminum oxide (Al_2O_3) [7,8], zinc oxide, iron oxide and their composites have been synthesized and characterized by various methods [9–11]. Graphene is a tremendously assorted material, and can be mixed with other elements (which includes gases and metals) to produce different materials with various advanced properties [12]. For instance, graphene oxide (GO) has been widely utilized in the development of various biosensors because of its exceptional properties including excellent water dispersibility, biocompatibility and large surface area [13,14]. Among a range of different nanomaterials, graphene possesses extraordinary structural, mechanical and physicochemical properties [15].

Another important carbon material is carbon nanotubes (CNTs), which are valuable for nanotechnology, electronics, optics and other fields of materials science and technology [16,17]. Structurally multi walled carbon nanotubes (MWCNTs) consist of several layers of graphite superimposed and they are rolled in on themselves to convert into a tubular shape [18]. The CNT and graphene with other metal nanoparticles gives an enhanced or synergetic effects in its properties [19]. Due to the higher stability and large surface area, graphene and CNT hybrid could be a better supporting material to attach the metal nanoparticles [20]. The chemical method is comparatively easy and inexpensive with negligible difficulties to place and align the consequential nanostructures in preferred configurations or patterns. Therefore, herein we utilized GO-MWCNT hybrid as a platform for the decoration of Pt nanoparticles via chemical reduction [21,22]. All these nanomaterials are used in the detection of glycated hemoglobin through enhanced electrochemistry.

Glycated hemoglobin (*hemoglobin A1c, A1C, HbA_{1c}* or *Hb_{1c}*; is also known as HGBA1C or HbA1c) is a form of hemoglobin which is considered primarily to identify the average plasma glucose concentration over extended or prolonged period of time [23]. It has been observed after it is formed in a non-enzymatic glycation pathway by hemoglobin's disclosure to plasma glucose. HbA1c is a computation of the beta-N-1-deoxy fructosyl component of hemoglobin [24]. HbA1c is defined as hemoglobin which is irretrievably glycated at one or both N-terminal valines of the beta

* Corresponding author. Tel.: +91 8130615833.
E-mail address: nidhichauhan2007@rediffmail.com (N. Chauhan).

http://dx.doi.org/10.1016/j.ijbiomac.2017.03.127
0141-8130/

chains [25]. HbA1c has been the mostly used and accepted test for monitoring the glycemic control in individuals with diabetes. Once a hemoglobin molecule is glycated, it continues to remain in the red blood cell for the rest of its life span (120 days). HbA1c laboratory tests are used to check the control in diabetes mellitus.

In this work, by combining the advantages of PtNPs, rGO and MWCNT nanohybrids were designed and synthesized for the detection of HbA1c. A novel ultrasensitive electrochemical biosensor was fabricated and characterized for the selective detection of HbA1c using fructosyl amino oxidase (FAO) enzyme. The application is toward determination of HbA1c in whole blood samples. The study can provide a promising platform for fabricating nanohybrid bioelectrode.

2. Experimental

2.1. Chemicals and reagents

Fructosyl-amino acid oxidase (FAO, EC:1.5.3, extracted from recombinant *E. coli*), Bovine serum albumin (BSA) and glutaraldehyde (GA) were procured from Sigma–Aldrich, St. Louis, USA. Graphite powder, hexachloroplatinic (IV) acid hydrate ($H_2PtCl_6{\cdot}xH_2O$), phenol, horseradish peroxidase, $NaNO_3$, H_2SO_4, $K_3Fe(CN)_6$ and $K_4Fe(CN)_6$ from Sisco Research Laboratory, Mumbai, India and gold wire (1.5 cm × 0.05 cm) (23 carat) were purchased from nearby market. Carboxylated multi-walled carbon nanotubes (MWCNT or MWCNT) (metal content: nil, 12 walls, length 15–30 mm, purity 95%) from Intelligent Materials Pvt. Ltd., Panchkula (Haryana), India, were used.

2.2. Preparation of substrate

The substrate for HbA1c i.e. fructosyl valine (FV) is not available commercially thus it was synthesized in our laboratory [26]. So 40 ml pyridine and 40 ml acetic acid were mixed together with L-valine (0.16 M, 1.88 g) and then stirred for 30 min at 25 °C. Afterwards, 4 g glucose (0.25 M) was added and purged by using nitrogen for 10 min and again stirred for 3 days at 25 °C. The dark colored product was separated out by filtering and the solvent was left for evaporation. By the process of re-crystallization in methanol, a yellowish amorphous product was obtained [26].

2.3. Preparation of graphene oxide

Graphene was synthesized by the modified Hummers method [27]. 3.33 g of natural graphite and 1.66 g of $NaNO_3$ were added to 76.66 ml of concentrated sulfuric acid under stirring in a flask immersed in an ice water bath. Then 10 g of $KMnO_4$ was added slowly and the mixture was stirred at 30 °C for 2 h. Next 153.33 ml of distilled water was added and the mixture was further stirred for 30 min at 95 °C. Finally, 313.33 ml of distilled water and 10 ml of H_2O_2 (5%) were subsequently added to terminate the reaction and the color of the solution turned from dark brown to yellow. The generated solid graphite oxide (GO) was separated by centrifugation then washed and lastly dried under vacuum [28]. This GO was further reduced to rGO by using hydrazine monohydrate.

2.4. Assembly of rGO–MWCNT hydrogel

The material was prepared by the addition of 2 mg of MWCNT to a 4 mg/ml homogenous rGO aqueous dispersion (the proportion of rGO to MWCNT was 2:1) under sonication for approximately 30 min. The mixture was subsequently sealed in a Teflon Lined Autoclave at 150 °C for 12 h. After the mixture was cooled in room temperature air with natural convection, a black gel like 3D cylinder substance was obtained. The size of the hydrogel could be freely adjusted by changing the volume of the rGO aqueous dispersion [29,30].

2.5. Biosensor fabrication

Piranha solution is prepared. It is a mixture which contains three parts of concentrated sulfuric acid and one part of 30% hydrogen peroxide solution in a ratio of 4:1. It should always be prepared by adding hydrogen peroxide to sulfuric acid very slowly, never in reverse [31]. Mixing the solution is extremely exothermic. For the preparation of rGO–MWCNT/Au electrode, 5.0 ml of rGO-MWCNT dispersion was used as electrolyte. A conventional three-electrode cell was used, including an Au as the working electrode, a Ag/AgCl electrode as the reference electrode, and platinum wire as the counter electrode. Cyclic voltammetry (CV) was performed by scanning between 0 and −1.0 V at a scan rate of 50 mV s^{-1} [32]. Then Au modified by rGO-MWCNT hybrids was taken off and rinsed with water three times lightly.

The electrochemical deposition of PtNPs was conducted using three-electrode system. The rGO-MWCNT/Au electrode was modified with PtNPs by using cyclic voltammogram with potential ranging from −0.2 to 0.7 V in a precursor solution consisting of 5 mM Potassium ferricyanide and K_2PtCl_6 for 10 cycles. The nanoparticles were controlled on the working electrode by changing the scan rate.

The glutaraldehyde (GA, 0.25 wt%), bovine serum albumin (BSA, 0.5 mgml^{-1}) and FAO (30 Uml^{-1}) were assorted together properly (all of these materials were dissolved in phosphate buffer, pH = 7.0), then they were allowed to drop onto an PtNPS/rGO–MWCNT/Au electrode with 5 μl of total amount. The biosensor will be achieved after the finish of cross-linking reaction during a period of stillness in a refrigerator at 4 °C (Scheme 1).

All the electrochemical analysis were performed by an potentiostat/galvanostat (Biologics, SP-150) with a typical three-electrode association composed of an Ag/AgCl (3 M KCl) reference electrode, a platinum auxiliary electrode and FAO/PtNPS/rGO–MWCNT/Au electrode as working electrode. We optimized all of parameters that robustly influenced the electrochemical performance of HbA1c. Simultaneously, the detection conditions like upper/lower limiting potential were also optimized.

2.6. The detection of HbA1c in whole blood samples through the fabricated biosensor

The healthy individuals and diabetes patients provided blood samples which were collected with EDTA as anticoagulant from Bio Diagnostics Laboratory, Rohini, New Delhi. In order to mix the blood cells, a mild inversion was applied. The mixing of 30 μl of whole blood in 300 μl of lysis buffer was carried out to check proper hemolysis and afterwards incubated for 10 min. Furthermore, the cells were lysed by using lysis buffer consisting 100 mM CHES (pH 8.7), 0.45% SDS, 1% Triton X-100 and 0.5 mM of Dess–Martin periodinane. A proteolytic digestion was performed of human blood samples by mixing of a solution including oxidizing agent (1 mM), 4 U/ml purified *Bacillus sp*. Proteases and 5 mM MES. This proteolytic digestion leads to the release of certain amino acids including glycated valines from the hemoglobin beta chains which then serves as substrates for the FAO and consequently produces H_2O_2 by combining 0.1 M sodium phosphate buffer (pH 7.5), 90 U/ml peroxidase and 0.8 mM of 4-amino anti pyrine which breaks N-terminal amino acids either histidine or valine [33,34]. The numbers of current produced for detection is principally based upon splitting of H_2O_2 released by the oxidation of substrate by immobilized enzyme (FAO), which is evidently proportional to the HbA1c concentration.

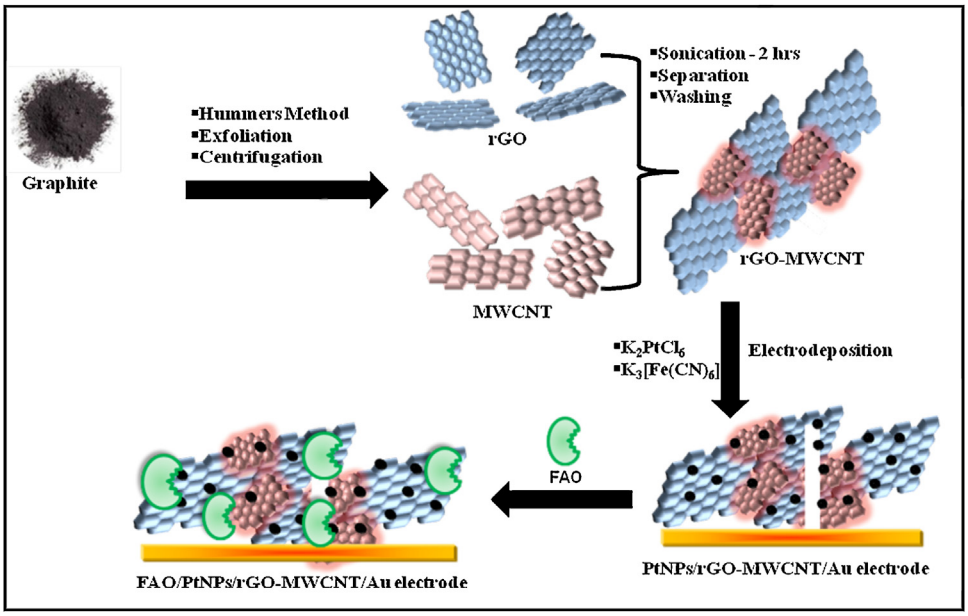

Scheme 1. Schematic illustration of the steps involved in the preparation of the FAO/PtNPs/rGO–MWCNT nanocomposite modified Au electrode.

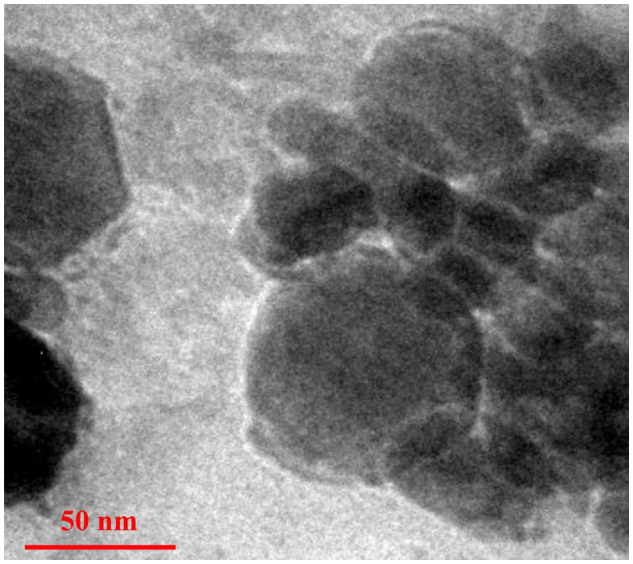

Fig. 1. TEM image of rGO nanoparticles.

Under the optimal conditions, the HbA1c values were calculated by the calibration/standard curve prepared for FV. Finally, the present (by biosensor) results were compared with the results obtained from the pathology lab using the standard HPLC method.

3. Results and Discussion

3.1. The morphology of nanomaterials and working electrode

Morphology and size distribution of the synthesized nanocomposites were perceived by means of TEM and SEM methods. Fig. 1 shows the TEM images of synthesized rGO in high magnification. The fabricated rGO disclosed a size of nearly 20–50 nm.

Fig. 2A portrays the XRD patterns of MWCNT (a), graphite (b), GO (c) and PtNPs/rGO–MWCNT (d). XRD patterns of MWCNTs and graphite exhibited a characteristic diffraction peak at 2θ of 26.17 Å (0 0 2), whereas it was completely disappeared in GO with appearance of new diffraction peak at 11.31, responsible for the large interlayer d-spacing (8.02 Å). XRD pattern of PtNPs/rGO–MWCNT shows the presence of new diffraction peaks at 40.371, 45.791, 67.531 and 81.071 ascribed to the fcc crystal structure of PtNPs. Moreover, disappearance of peak at 11.31 indicates the successful reduction of GO to rGO.

FTIR spectra for GO (a), rGO (b), rGO/MWCNT (c) and PtNPs/rGO–MWCNT (d) are shown in Fig. 2B. For GO (Curve a), the board stretching vibrations for O—H peak centered at 3265 cm^{-1} were recorded. The peaks at 1727, 1623, 1367, and 1056 were assigned to C—O stretching, C—C stretching bands for aromatic rings and O—H bending, C—OH stretching and C—O—C stretching, respectively. Furthermore, the peaks at 1041 and 1161 cm^{-1} were related to C—O vibration of alkoxy or epoxy groups [35]. The peak at 32,670 cm^{-1} in the rGO spectrum is attributed to O—H group that is obviously shows the reduction of O—H groups in compare to GO by using hydrothermal and the bands at 1358 and 1610 cm^{-1} are related to C—OH and C—O, respectively (Curve b). The peak 1025 cm^{-1} in the rGO spectrum are recognized as the C—O stretching vibration of the epoxy and alkoxy groups [36]. The existence of MWCNT in the composite could also be confirmed using FTIR spectroscopy (Curve c). A band centered at 1599 cm^{-1} and a shoulder at 1350 cm^{-1} were due to C=C stretching vibrations, while the band at 1117 cm^{-1} was associated with C—O stretching vibrations [37]. For the PtNPs/rGO–MWCNT nanocomposite (Curve d), the peaks at 1066, 1642, 1418, 2853, and 2925 cm^{-1} were assigned to C—O stretching vibrations, C=C stretching bands for aromatic rings and O—H bending, O—H deformation, as well as symmetric and asymmetric stretching vibrations of CH_2 groups, respectively [38]. The broad peak of 3300 cm^{-1} for PtNPs/rGO–MWCNT nanocomposite could be attributed to O—H stretching vibrations of the absorbed water molecules [38]. The O—H peak of rGO dramatically reduced compared to the board stretching vibrations O—H peak of GO centered at 3265 cm^{-1} (Curve a) caused by hydrothermal reduction.

The morphologies of bare Au electrode (image a), PtNPs/rGO–MWCNT/Au electrode (image b) and FAO/PtNPs/rGO–MWCNT/Au electrode (image c) were characterized by scanning electron microscope (SEM). The surface of the Au electrode (Fig. 3) was predominated by uniform and smooth shaped layer. In Fig. 3 (image b), PtNPs were uniformly distributed in the rGO–MWCNT matrix and covering the surface of

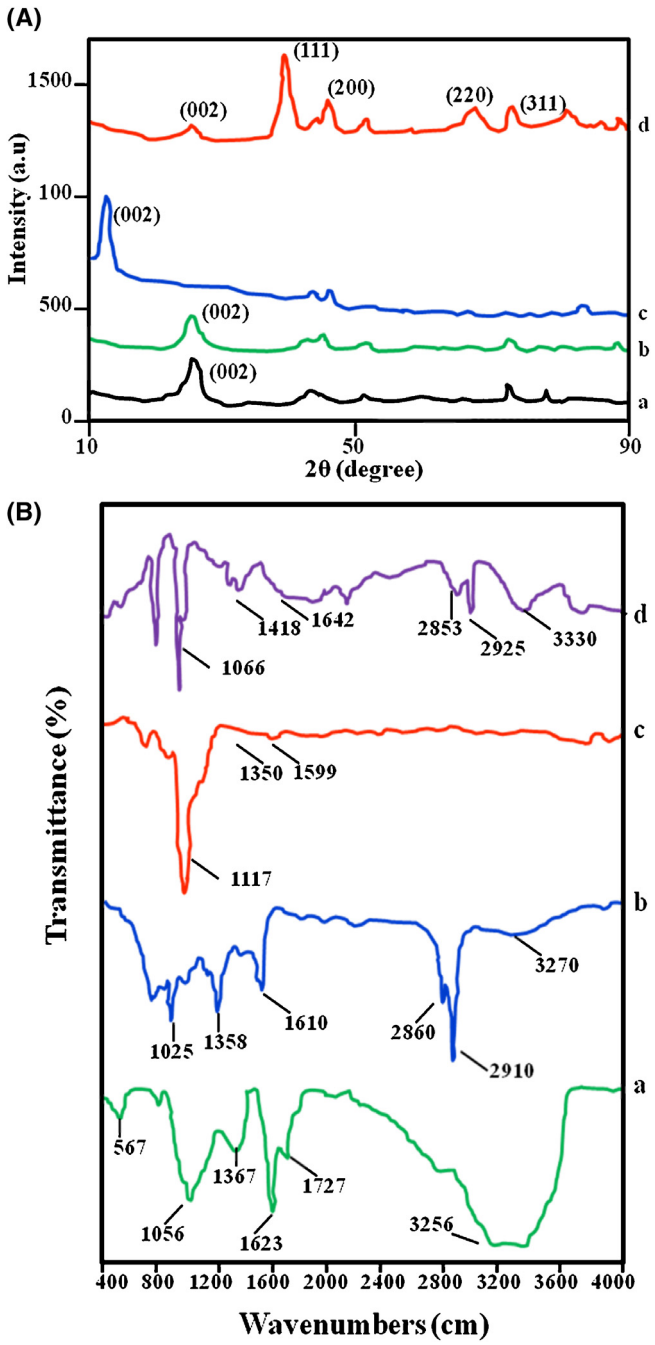

Fig. 2. A) XRD patterns of MWCNTs (a), graphite (b), GO (c) and PtNPs/rGO–MWCNT (d). B) FTIR spectra of GO (a), rGO (b), MWCNT (c) and PtNPs/rGO–MWCNT (d).

the MWCNTs, resulting in the formation of homogenous, tubular network structure. Note that the formation of fairly homogeneous GO structure and MWCNTs network can still be seen in image (b). This 3D porous network structure of rGO–MWCNT–Pt nanocomposite not only could increase the current response, but also provides more exposed active sites for Pt nucleation. Moreover, presence of globular morphology as indicated by circle in Fig. 3 (image c) depicts immobilization of FAO on the surface of PtNPs/rGO–MWCNT/Au electrode. The spherical, tubular and folded surface of PtNPs/rGO–MWCNT nanocomposites provides a large rough surface area for enhanced loading of enzyme.

EDX spectrum of rGO–MWCNT–Pt nanocomposite portrays the signals of gold, carbon, oxygen and platinum with weight percentage of 56.11, 23.7, 7.8 and 12.39%, respectively. The existence of Pt signal along with carbon and oxygen proved the formation of Pt nanoparticles onto the rGO–MWCNT modified Au electrode (Fig. 3, image d).

3.2. Cyclic voltammetry studies of various stages for the fabrication of working electrode

Fig. 4A shows the characteristics CV studies of bare Au electrode, rGO–MWCNT/Au electrode, PtNPs/rGO–MWCNT/Au electrode and FAO/PtNPs/rGO–MWCNT/Au electrode in $[Fe(CN)_6]^{3-/4-}$ electrolyte containing 0.5 mM sodium phosphate buffer (pH 7.4) at scan rate of 50 mVs^{-1} from potential −0.2–0.4 V. Anodic peak current (Ipa) values of bare Au electrode, rGO–MWCNT/Au electrode and PtNPs/rGO–MWCNT/Au electrode are found to be as 0.002, 0.07 and 0.11 mA, respectively as shown in Fig. 4A. Increase of oxidation peak current value from 0.07 mA to 0.11 mA confirms electrodeposition of highly conductive PtNPs film onto rGO–MWCNT/Au electrode surface. The large increase in peak current is associated with enhanced electroactive surface area and facile heterogeneous electron transfer properties of rGO–MWCNT composites leading to the large-scale redox conversion [39]. After immobilization of FAO enzyme on PtNPs/rGO–MWCNT/Au electrode, magnitude of current (0.05 mA) was found to be decreased because of inherent insulating nature of bulky enzyme molecules which acts as a barrier for electron transport [40].

3.3. Impedance study

Fig. 4B shows Nyquist plots obtained for all electrodes: bare Au electrode, PtNPs/rGO–MWCNT/Au electrode and FAO/PtNPs/rGO–MWCNT/Au electrode measured in $[Fe(CN)_6]^{3-/4-}$ electrolyte containing 0.5 mM sodium phosphate buffer (pH 7.4), scanned in the frequency range from 0.01 to 1×10^5 Hz at potential of 5 mV. The semicircular part seen at higher frequencies corresponds to the electron transfer limited process and its diameter is equal to the charge transfer resistance (Rct), i.e. resistance provided by the electrode material to transfer charge from solution to the electrode, which is correlated to the modification of surface.

The values of Rct for bare Au electrode, PtNPs/rGO–MWCNT/Au electrode and FAO/PtNPs/rGO–MWCNT/Au electrode are 9.5, 2.5 and 5.8 kΩ, respectively. This reflects that the conductivity of the electrodes follows in the given order e.g., PtNPs/rGO–MWCNT/Au electrode > FAO/PtNPs/rGO–MWCNT/Au electrode > Au electrode. The enhanced charge transfer rate of PtNPs/rGO–MWCNT is due to the high electron mobility via the aromatic Π conjugated ring structure of the rGO modified electrode which facilitates diffusion of the negatively charged $[Fe(CN)_6]^{4-/3-}$ ions toward the electrode surface. After the immobilization of enzyme (FAO) on the surface of PtNPs/rGO–MWCNT/Au electrode, value of Rct is increased to 5.8 kΩ, indicating successful immobilization of FAO as confirmed by CV (Fig. 4A). The insulating nature of the enzymes diminishes conductivity of the bioelectrode as compared to the PtNPs/rGO–MWCNT/Au electrode [41].

3.4. Biosensing response characteristics

Fig. 5A illustrates the CV curves obtained for the FAO/PtNPs/rGO–MWCNT/Au electrode with varying concentrations of FV (substrate) in the solution of $[Fe(CN)_6]^{3-/4-}$ electrolyte containing 0.5 mM sodium phosphate buffer (pH 7.4). The peak oxidation current was observed which continuously increases with consecutive addition of substrate ranging from 0.05 to 1000 μM. Fig. 5A CV presents a pair of well-defined and symmetric redox peaks of $Fe(CN)_6]^{3-}/Fe(CN)_6]^{4-}$ on FAO/PtNPs/rGO–MWCNT/Au electrode in presence of various

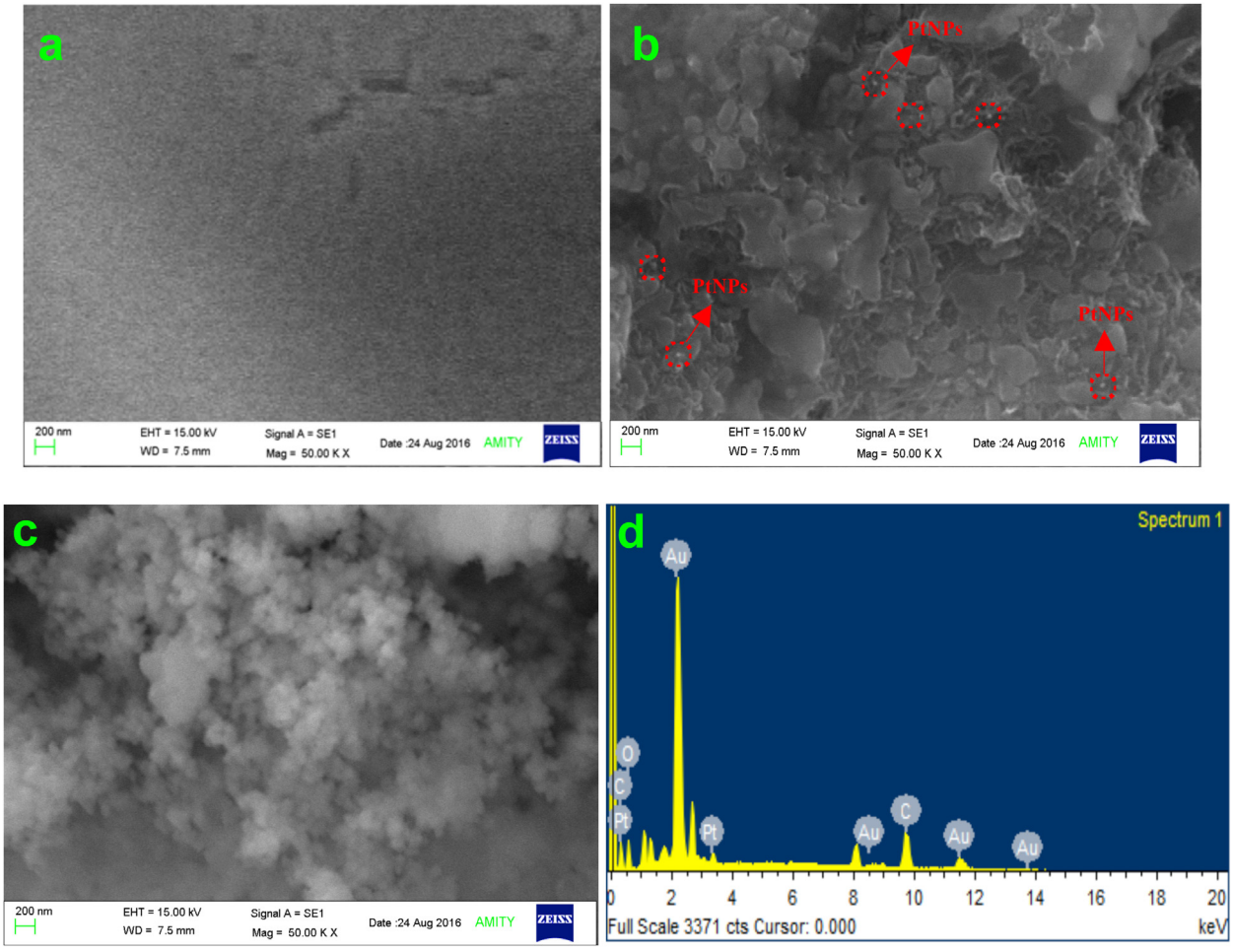

Fig. 3. SEM micrograph image of (a) bare Au electrode, (b) PtNPs/rGO–MWCNT/Au electrode and (c) FAO/PtNPs/rGO–MWCNT/Au electrode.

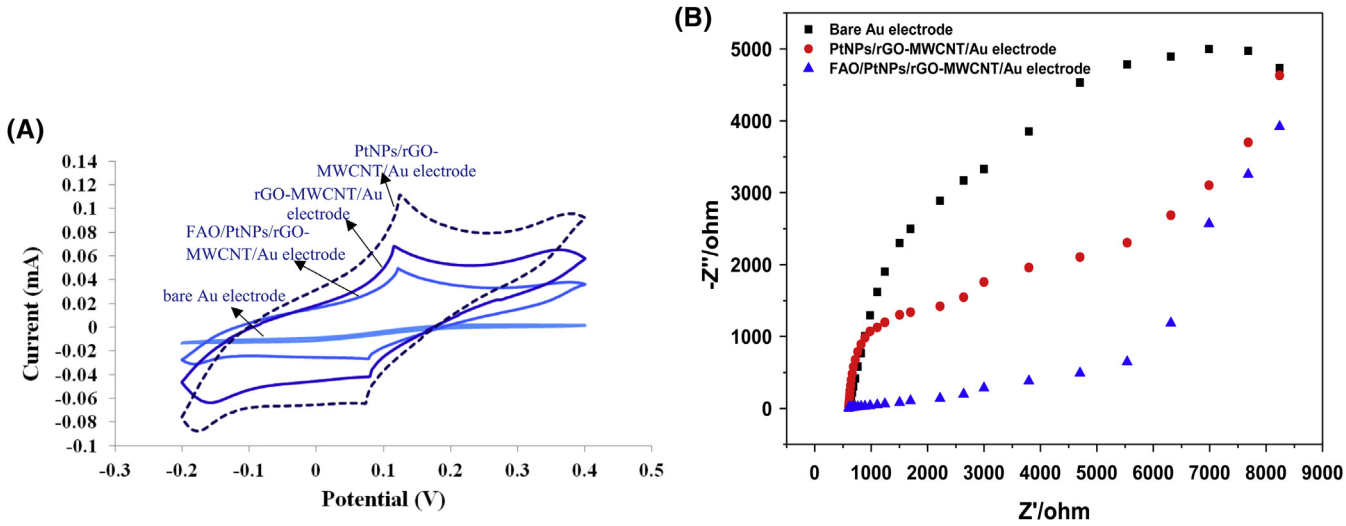

Fig. 4. A) CV curves of bare Au electrode, rGO–MWCNT/Au electrode, PtNPs/rGO–MWCNT/Au electrode and FAO/PtNPs/rGO–MWCNT/Au electrode obtained with $[Fe(CN)_6]^{3-/4-}$ electrolyte containing 0.5 mM sodium phosphate buffer (pH 7.4) at 50 mVs^{-1}. B) Electrochemical impedance plots (Nyquist plots) of the different electrodes: (a) bare Au electrode, (b) PtNPs/rGO–MWCNT/Au electrode and (c) FAO/PtNPs/rGO–MWCNT/Au electrode in $[Fe(CN)_6]^{3-/4-}$ electrolyte containing 0.5 mM sodium phosphate buffer (pH 7.4). The frequency range is between 0.01 and 100,000 Hz with amplitude of 5 mV.

concentration of FV (0.05–1000 μM). It is important to note that the potential difference (ΔE between Epa and Epc) and peak current ratio (Ipa/Ipc) of the FAO/PtNPs/rGO–MWCNT/Au electrode in presence of FV in sodium phosphate buffer (pH 7.4) are +0.14 and −0.08 confirm a reversible behavior of the electrode in presence of analyte (FV) [42]. The limit of detection of the present biosensor/FAO/PtNPs/rGO–MWCNT/Au electrode was measured upto 0.1 μM.

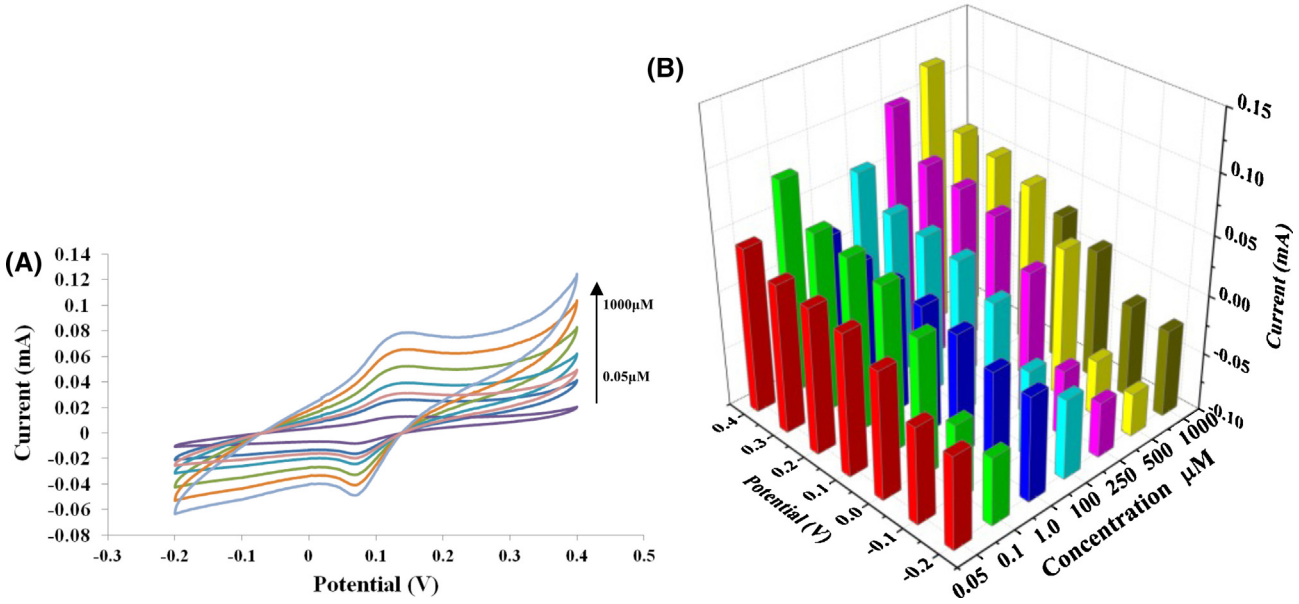

Fig. 5. A) Biosensing response studies (CV) of FAO/PtNPs/rGO–MWCNT/Au electrode with different FAO concentrations at 50 mVs^{-1} between −0.2 and +0.4 V in $[Fe(CN)_6]^{3-/4-}$ electrolyte containing 0.5 mM sodium phosphate buffer (pH 7.4). B) 3D representation of the cyclic voltammogram data at FAO/PtNPs/rGO–MWCNT/Au electrode for different substrate concentrations.

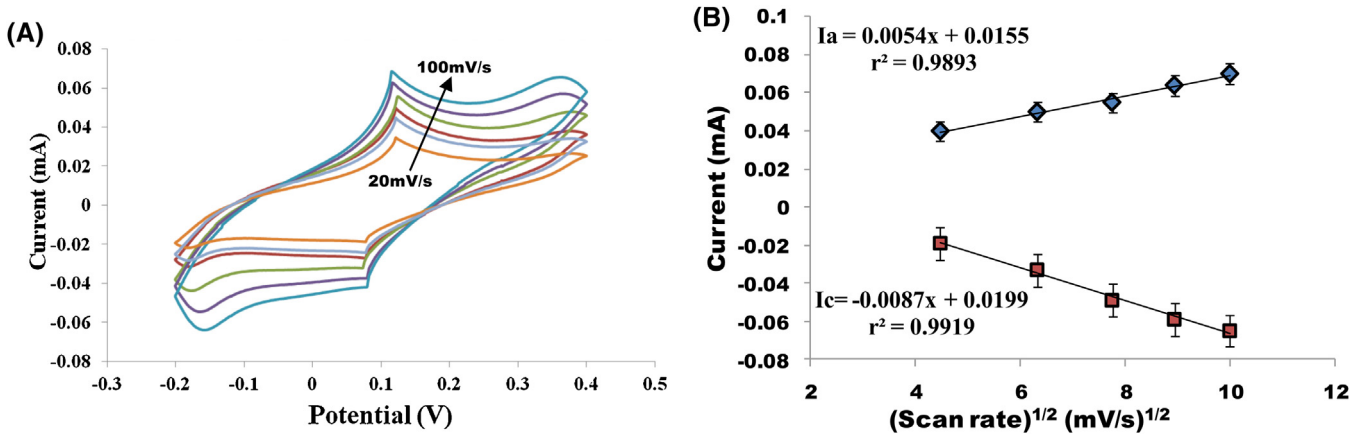

Fig. 6. A) The CV of FAO/PtNPs/rGO–MWCNT/Au electrode scanned in $[Fe(CN)_6]^{3-/4-}$ electrolyte containing 0.5 mM sodium phosphate buffer (pH 7.4) with 100 µM FV at different scan rates from 20 to 100 mVs^{-1}. B) The dependency of peak currents on variation of peak oxidation (Ipa) and reduction(Ipc) as a function of square root of scan rate.

Fig. 5B: presents the 3D plot for FAO/PtNPs/rGO–MWCNT/Au electrode at different FV concentrations. With increasing concentration of FV from 0.05 to 1000 µM, the peak current was gradually increased. Each experiment is repeated for three times to confirm the reproducibility. This constructed enzyme electrode can detect FV in the range of 0.05–1000 µM with low response time of 3 s. Response time was calculated on the basis of the time taken to reach the optimum current when FAO/PtNPs/rGO–MWCNT/Au electrode was exposed to 100 µM in the $[Fe(CN)_6]^{3-/4-}$ electrolyte containing 0.5 mM sodium phosphate buffer (pH 7.4). The value of sensitivity calculated from linear region of the calibration curve is 0.562 mA/µM.

The relationship between the current with potential of peak and respective scan rates gives important information about the electrochemical mechanism of the electrode process. Fig. 6A represents the obtained CVs on the FAO/PtNPs/rGO–MWCNT/Au electrode at various scan rates in 0.5 mM sodium phosphate buffer (pH 7.4). The recorded CVs show that the corresponding redox peak currents due to the behavior of FV with increasing scan rate from 20 to 100 mVs^{-1}. The scan rate 100 mVs^{-1} was selected as the best scan rate for further experiments. Considering the above scan rate, which has a sharp redox peaks can be seen very clearly, even though less current was observed in comparison to 20–80 mVs^{-1} scan rates. As seen in Fig. 6B, the redox peak current is directly proportional to the square root of scan rates between 10 and 100 mVs^{-1}. This behavior demonstrates that the redox process is a diffusion-controlled one. The plot between I and $\sqrt{}$scan rate can be expressed as:

$$Ipa\,(anodic) = 0.0054x + 0.0155\,(r^2 = 0.9893)$$

$$Ipc\,(cathodic) = 0.0087x + 0.0199\,(r^2 = 0.9919)$$

The apparent Michaelis–Menten Kinetic parameters ($K_{app}m$) of the enzymatic reaction, that determines the affinity of enzyme with the bio-analyte, is estimated using Hanes plot i.e. a plot between reciprocal of current response and inverse of analyte concentration. The $K_{app}m$ value for the immobilized enzyme is found to be as 7.5 µM, which is much lower than previously reported values (1660 and 987 µM) [43,44]. The low $K_{app}m$ further signifies that

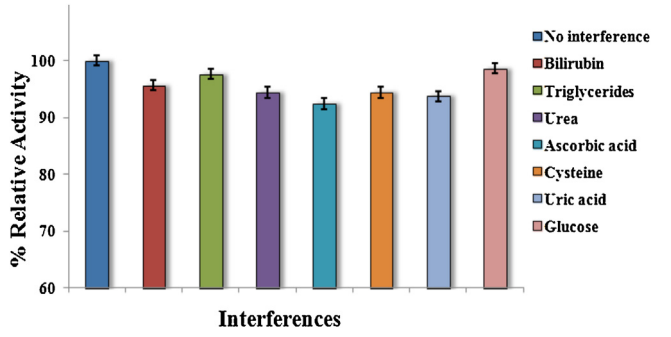

Fig. 7. Plot of interferents studies of FAO/PtNPs/rGO–MWCNT/Au electrode with 100 μM FV in 0.5 mM sodium phosphate buffer (pH 7.4).

FAO/PtNPs/rGO–MWCNT/Au electrode offers a favorable microenvironment toward enzymes for their biochemical interaction with analyte.

The optimum response of FAO/PtNPs/rGO–MWCNT/Au electrode is achieved at 7.4 pH and 30 °C. Therefore, the entire experiments were carried out at pH 7.4 and 30 °C. The analytical recoveries of added substrate in blood at levels of 0.2 and 0.4 μM were 93.7 and 98.3% respectively. Thus, the recovery was obtained satisfactorily with the present biosensor. Within and between batch coefficients of variation for the determination of HbA1c in blood on the same day and after one week of storage were 1.08 and 1.70%, respectively, suggesting sufficient precision and high accuracy.

The interfering substances at their physiological concentrations including bilirubin, triglycerides, urea, ascorbic acid, cysteine, uric acid and glucose were analyzed using current biosensor at 0.2 V versus Ag/AgCl in sodium phosphate buffer at pH 7.4. Negligible interference was noticed which is calculated by decrease in percentage of biosensor response in the presence of these substances showing 4.36% for bilirubin, 2.41% for triglycerides, 5.63% for urea, 7.65% for ascorbic acid, 5.6% for cysteine, 6.27% for uric acid and 1.42% for glucose (Fig. 7).

3.5. Application of the biosensor in real samples

To estimate the HbA1c from clinical sample using FAO/PtNPs/rGO–MWCNT/Au electrode, human whole blood samples were collected from a pathological lab (Bio Diagnostics lab, Rohini) located in Delhi. The FAO/PtNPs/rGO–MWCNT/Au electrode was dipped in the solution of sodium phosphate buffer (0.5 mM, pH 7.4) containing 5 mM $[Fe(CN)_6]^{3-/4-}$ and 100 μl blood samples at of 50 mVs^{-1} and response current was noted. The values of HbA1c in blood samples, as estimated from the calibration curve using FAO/PtNPs/rGO–MWCNT/Au electrode are harmonizing with clinical values (Tables 1 and 2). The results suggested that the HbA1c in human blood samples determined by using the methods developed in this study is an acceptable agreement with the results determined using HPLC methods in a diagnostic laboratory.

3.6. Storage stability of the working electrode

The shelf life of the FAO/PtNPs/rGO–MWCNT/Au electrode was investigated by measuring the amperometric response current in the presence of 100 μM standard FV solution in PBS at a regular interval of a gap of 7 days. It is observed that the constructed bioelectrode retains its enzyme activity up to 90% up to 12 weeks, when stored under refrigerated conditions (4 °C). For comparison, the CV of PtNPs/rGO–MWCNT/Au was studied simultaneously in buffer at a regular interval of a gap of 7 days and observed that the electrode was stable upto 15 weeks without significant loss in response current. The loss of activity of bioelectrode was caused by denaturing of the enzymes indicating a stability of PtNPs/rGO–MWCNT.

Table 1
HbA_{1c} levels of apparently healthy persons, as measured by FAO/PtNPs/rGO–MWCNT/Au electrode based biosensor.

S.No.	Age (y)	Gender[a]	% HbA1c by FAO/PtNPs/rGO–MWCNT/Au electrode
1.	32	F	4.5
2.	34	M	4.2
3.	40	M	4.6
4.	35	F	4.4
5.	37	F	4.2
6.	44	M	5.1
7.	52	F	5.8
8.	49	F	5.2
9.	51	F	5.2
10.	39	M	4.7

[a] M: male; F: female.

Table 2
HbA_{1c} levels of diabetic patients, as measured by FAO/PtNPs/rGO–MWCNT/Au electrode based biosensor.

S.No.	Age (y)	Gender[a]	% HbA1c by FAO/PtNPs/rGO–MWCNT/Au electrode
1.	45	F	8.6
2.	35	M	6.5
3.	41	F	7.5
4.	49	F	8.8
5.	53	M	9.6
6.	46	F	7.9
7.	37	F	7.3
8.	57	F	9.2
9.	44	M	8.1
10.	54	M	7.8

[a] M: male; F: female.

4. Conclusions

This work shows that novel PtNPs/rGO-MWCNT nanocomposites were successfully synthesized in a facile manner and further applied to construct electrochemical sensing system. It is found that the synthetic 3D hybrid nanostructure shows excellent electrocatalytic activity toward the oxidation of FV by significantly enhancing the peak currents. Moreover, the results obtained from application of the proposed sensor for determining HbA1c in whole blood samples confirmed very good accuracy, selectivity, sensitivity, precision and reliability of our approach. The results of response studies reveal that this enzyme modified electrode can detect FV in a wide concentration range of 0.05–1000 μM with low detection limit (0.2 μM), high sensitivity 0.562 mA/μM and low response time of 3 s. The present electrode is successfully employed to detect HbA1c from blood samples and shows a shelf life of about 12 weeks with negligible interference. Considering the reliability, stability and performance of proposed HbA1c biosensor, it can be concluded that FAO/PtNPs/rGO–MWCNT/Au electrode has a promising future in clinical diagnosis.

In summary, the proposed method exhibits excellent advantages of low cost, good stability and super sensing performances, illustrating that PtNPs/rGO-MWCNT nanocomposites can be a promising candidate for generating sensitive and selective electrochemical sensing and other catalytic applications.

Acknowledgments

Our work gratefully acknowledged the support from Science and Engineering Research Board (SERB), New Delhi under the Young Scientist Scheme (Fast Track; File No. SB/YS/LS_106/2013).

References

[1] A. Kaushik, A. Vasudev, S.K. Arya, S. Bhansali, Mediator and label free estimation of stress biomarker using electrophoretically deposited Ag@AgO-polyaniline hybrid nanocomposite, Biosens. Bioelectron. 50 (2013) 35–41.
[2] P. Jiang-feng, Z. Feng-Qi, S. Xiu-duo, Z. Wei, Progress of the application of light weight carbon materials and their composites in solid rocket propellants, Chin. J. Explos. Propellants 2 (2014) 1–6.
[3] M. Goudarzi, N. Mir, M. Mousavi-Kamazani, S. Bagheri, M. Salavati-Niasari, Biosynthesis and characterization of silver nanoparticles prepared from two novel natural precursors by facile thermal decomposition methods, Sci. Rep. 6 (2016) 32539.
[4] M. Goudarzi, M. Salavati-Niasari, M. Motaghedifard, S.M. Hosseinpour-Mashkani, Semiconductive Tl_2O_3 nanoparticles: facile synthesis in liquid phase, characterization and its applications as photocatalytic substrate and electrochemical sensor, J. Mol. Liq. 219 (2016) 720–727.
[5] M. Goudarzi, M. Salavati-Niasari, Controllable synthesis of new Tl2S2O3 nanostructures via hydrothermal process; characterization and investigation photocatalytic activity for degradation of some anionic dyes, J. Mole. Liq. 219 (2016) 851–857.
[6] M. Goudarzi, M. Salavati-Niasari, M. Bazarganipour, M. Motaghedifard, Sonochemical synthesis of Tl_2O_3 nanostructures: supported on multi-walled carbon nanotube modified electrode for monitoring of copper ions, J. Mater. Sci. Mater. Electron. 27 (4) (2016) 3675–3682.
[7] M. Goudarzi, Z. Zarghami, M. Salavati-Niasari, Novel and solvent-free cochineal-assisted synthesis of Ag–Al_2O_3 nanocomposites via solid-state thermal decomposition route: characterization and photocatalytic activity assessment, J. Mater. Sci. Mater. Electron. 27 (2016) 9789–9797.
[8] M. Goudarzi, D. Ghanbari, M. Salavati-Niasari, A. Ahmadi, Synthesis and characterization of $Al(OH)_3$, Al_2O_3 nanoparticles and polymeric nanocomposites, J. Cluster Sci. 27 (2016) 25–38.
[9] M. Goudarzi, M. Bazarganipour, M. Salavati-Niasari, Synthesis, characterization and degradation of organic dye over Co_3O_4 nanoparticles prepared from new binuclear complex precursors, RSC Adv. 4 (2014) 46517–46520.
[10] M. Goudarzi, D. Ghanbari, M. Salavati-Niasari, Photo-catalyst thallium sulfide: synthesis and optical characterization different morphologies of Tl_2S nanostructures, J. Mater. Sci. Mater. Electron. 26 (2015) 8798–8806.
[11] S.F. Moustafa, W.M. Daoush, Synthesis of nano-sized Fe-Ni powder by chemical process for magnetic applications, J. Mater. Process. Technol. 181 (2007) 59–63.
[12] K.S. Subrahmanyam, K.M. Arun, S.K. Pati, C.N.R. Rao, A study of graphene decorated with metal nanoparticles, Chem. Phys. Lett. 497 (2010) 70–75.
[13] N. Chauhan, R. Rawal, V. Hooda, U. Jain, Electrochemical biosensor with graphene oxide nanoparticles and polypyrrole interface for the detection of bilirubin, RSC Adv. 6 (2016) 63624–63633.
[14] N. Chauhan, J. Narang, U. Jain, Highly sensitive and rapid detection of acetylcholine using platinum-graphene nanoparticles modified ITO plate, Analyst 140 (2015) 1988–1994.
[15] N. Xia, L. Liu, Z. Sun, B. Zhou, Nanocomposites of graphene with ferrocene or hemin: preparation and application in electrochemical sensing, J. Nanomater. 2015 (2015), Article ID 892674, 9 pages.
[16] A. Bianco, K. Kostarelos, M. Prato, Applications of carbon nanotubes in drug delivery, Curr. Opin. Chem. Biol. 9 (2005) 674–679.
[17] R. Rawal, S. Chawla, N. Chauhan, T. Dahiya, C.S. Pundir, Construction of amperometric uric acid biosensor based on uricase immobilized on PBNPs/c-MWCNT/PANI/Au nanocomposite, Int. J. Biol. Macromol. 50 (2012) 112–118.
[18] R.Y. Zhang, X.M. Wang, One step synthesis of multiwalled carbon nanotube/gold nanocomposites for enhancing electrochemical response, Chem. Mater. 19 (2007) 976–978.
[19] Y. Wang, C.Y. Bi, A novel nitrite biosensor based on direct electron transfer of hemoglobin immobilized on a graphene oxide/Au nanoparticles/multiwalled carbon nanotubes nanocomposite film, RSC Adv. 4 (2014) 31573–31580.
[20] J. Shi, H. Zhang, A. Snyder, M. Wang, J. Xie, D.M. Porterfield, L.A. Stanciu, An aqueous media based approach for the preparation of a biosensor platform composed of graphene oxide and Pt-black, Biosens. Bioelectron. 38 (2012) 314–320.
[21] Y. Sun, K. He, Z. Zhang, A. Zhou, H. Duan, Real-time electrochemical detection of hydrogen peroxide secretion in live cells by Pt nanoparticles decorated graphene-carbon nanotube hybrid paper electrode, Biosens. Bioelectron. 15 (2015) 358–364.
[22] Z. Wen, S. Ci, J. Li, Pt nanoparticles inserting in carbon nanotube arrays: nanocomposites for glucose biosensors, J. Phys. Chem. C 113 (2009) 13482–13487.
[23] K. Miedema, Standardization of HbA1c and optimal range of monitoring, Scand. J. Clin. Lab. Invest. 240 (2005) 61–72.
[24] K.P. Peterson, J.G. Pavlovich, D. Goldstein, R. Little, J. England, C.M. Peterson, What is hemoglobin A1c? an analysis of glycated hemoglobins by electrospray ionization mass spectrometry, Clin. Chem. 44 (1998) 1951–1958.
[25] U. Kobold, J.O. Jeppsson, T. Dulffer, A. Finke, W. Hoetzel, K. Miedema, Candidate reference method for hemoglobin A1c based on peptide mapping, Clin. Chem. 43 (1997) 1944–1951.
[26] R. Rajkumar, A. Warsinke, H. Mohwald, F.W. Scheller, M. Katterle, Development of fructosyl valine binding polymers by covalent imprinting, Biosens. Bioelectron. 22 (2007) 318–325.
[27] W.S. Hummers, R.E. Offeman, Preparation of graphitic oxide, J. Am. Chem. Soc. 80 (1958), 1339-1339.
[28] Y. Zhou, Q.L. Bao, L.A. Tang, Y.L. Zhong, K.P. Loh, Hydrothermal dehydration for the “green” reduction of exfoliated graphene oxide to graphene and demonstration of tunable optical limiting properties, Chem. Mater. 21 (2009) 2950–2956.
[29] S.W. Ting, A.P. Periasamy, S.M. Chen, R. Saraswathi, Direct electrochemistry of catalase immobilized at electrochemically reduced graphene oxide modified electrode for amperometric H2O2 biosensor, Int. J. Electrochem. Sci. 6 (2011) 4438–4453.
[30] K.S. Novoselov, V.I. Falko, L. Colombo, P.R. Gellert, M.G. Schwab, K. Kim, A roadmap for grapheme, Nature 490 (2012) 192–200.
[31] T. Sun, Z. Zhang, J. Xiao, C. Chen, F. Xiao, S. Wang, Y. Liu, Facile and green synthesis of palladium nanoparticles graphene carbon nanotube material with high catalytic activity, Sci. Rep. 3 (2013), 2527-2527.
[32] Y. Zhang, Y. Ji, Z. Wang, S. Liu, T. Zhang, Electrodeposition synthesis of reduced graphene oxide carbon nanotube hybrids on indium tin oxide electrode for simultaneous electrochemical detection of ascorbic acid, dopamine and uric acid, RSC Adv. 5 (2013) 106307–106314.
[33] S. Liu, H. Ju, Reagentless glucose biosensor based on direct electron transfer of glucose oxidase immobilized on colloidal gold modified carbon paste electrode, Biosens. Bioelectron. 19 (2003) 177–183.
[34] S. Aboutalebi, A. Chidembo, M. Salari, K.K. Konstantinov, D. Wexler, H.K. Liu, S.X. Dou, Comparison of GO, GO/MWCNTs composite and MWCNTs as potential electrode materials for supercapacitors, Energy Environ. Sci. 4 (2011) 1855–1865.
[35] V.H. Pham, T.V. Cuong, S.H. Hur, E. Oh, E.J. Kim, E.W. Shin, J.S. Chung, Chemical functionalization of graphene sheets by solvothermal reduction of a graphene oxide suspension in N-methyl-2-pyrrolidone, J. Mater. Chem. 21 (2011) 3371–3377.
[36] M. Li, X. Bo, Z. Mu, Y. Zhang, L. Guo, Electrodeposition of nickel oxide and platinum nanoparticles on electrochemically reduced graphene oxide film as a nonenzymatic glucose sensor, Sens. Actuators B: Chem. 192 (2014) 261–268.
[37] P. Dubey, D. Muthukumaran, S. Dash, R. Mukhopadhyay, S. Sarkar, Synthesis and characterization of water-soluble carbon nanotubes from mustard soot, Pramana 65 (2005) 681–697.
[38] C. Cheng, S. Nie, S. Li, H. Peng, H. Yang, L. Ma, S. Sun, C. Zhao, Biopolymer functionalized reduced graphene oxide with enhanced biocompatibility via mussel inspired coatings/anchors, J. Mater. Chem. B 1 (2013) 265–275.
[39] J. Chen, X. Zheng, F. Miao, J. Zhang, X. Cui, W. Zheng, A polyaniline microtubes platform for direct electron transfer of glucose oxidase and biosensing applications, J. Appl. Electrochem. 42 (2012) 875–881.
[40] V. Mani, D. Bose, S.M. Chena, S. Ramiah, Direct electrochemistry of myoglobin at reduced graphene oxide multiwalled carbon nanotubes platinum nanoparticles nanocomposite and biosensing towards hydrogen peroxide and nitrite, Biosens. Bioelectron. 53 (2014) 420–427.
[41] K. Wang, H.N. Li, J. Wu, C. Ju, J.J. Yan, Q. Liu, B. Qiu, TiO_2-decorated graphene nanohybrids for fabricating an amperometric acetylcholinesterase biosensor, Analyst 136 (2011) 3349–3354.
[42] B. Liang, L. Lang, G. Yang, Y. Hu, X. Guo, X. Ye, Current trends in nanomaterial-based amperometric biosensors, Biosens. Bioelectron. 43 (2014) 131–136.
[43] S. Chawla, C.S. Pundir, An electrochemical biosensor for fructosyl valine for glycosylated hemoglobin detection based on core–shell magnetic bionanoparticles modified gold electrode, Biosens. Bioelectron. 26 (2011) 3438–3443.
[44] L. Fang, W. Li, Y. Zhou, C.C. Liu, A single use, disposable iridium-modified electrochemical biosensor for fructosyl valine for the glycoslated hemoglobin detection, Sens. Actuator B 137 (2008) 235–238.